Genetic Algorithm Based Dynamics Modeling and Control of a Parallel Rehabilitation Robot

Chen Wang*‡, Liang Peng*, Lincong Luo*‡, Zeng-Guang Hou*†, Weiqun Wang*
*State Key Laboratory of Management and Control for Complex Systems, Institute of Automation, Chinese Academy of Sciences, Beijing 100190, China;
†CAS Center for Excellence in Brain Science and Intelligence Technology, Beijing 100190, China;
‡University of Chinese Academy of Sciences, Beijing 100049, China.

***Abstract*—This paper is devoted to modeling and controlling a new upper-limb rehabilitation robot which has a parallel structure. Genetic algorithm (GA) is successfully applied in parameter identification based on dynamic analysis of the parallel robot. For accurate identification, joint velocities and accelerations are computed by the Kalman filter. By taking the non-linear characteristics of frictions into account, the unknown friction parameters differ depending on directions of motion. Compared with the traditional least square estimation (LSE) based method, the proposed identification method improves performance. Further, a model-based PD computed-torque controller is designed, and the feasibility of the estimated dynamic model and controller is validated by passive training task along a circular trajectory.**

I. Introduction

During the last decade, stroke has become the second leading cause of death over the world, according to statistics from WHO (World Health Organization). Most stroke survivors are left with severe disabilities, mainly motor impairments on upper-limb movements, which affect their performances in ADLs (activities of daily living) [1]. For these patients, long-term and high-intensity rehabilitation can help to restore the motor functionality as a consequence of inducing neural plasticity. While intense repetitions of motor activities impose a significant burden for therapists, robot-aided therapy is believed to be a promising method for rehabilitation training. On one hand, robots can guarantee training intensity, and can interact with the patient to "coach" them in the home environment. On the other hand, robot therapy can achieve more therapy modes to increase the patient's training motivation.

Different from versatile industrial robots, rehabilitation robots focus on safety performance and compliant interaction features rather than manipulation accuracy. In order to assist patients in completing movements while remaining complaint, rehabilitation robots typically adopt model-based and adaptive control approach [2]. The performance of the advanced robot controller, such as computed torque depends directly on the model accuracy. However, the dynamic model of the robot contains uncertainties in many parameters, and it reduces interaction transparency between human and the robot.

Fig. 1. The upper-limb rehabilitation robot.

Dynamic identification methods have gained importance for developing model-based controllers. Because of the complexity of rehabilitation robots, it is impractical to obtain the robot models by direct measurement. Experimental robot identification is the only efficient way to obtain accurate robot models as well as indications on their accuracy, confidence and validity [3]. Moreover, reliable robot identification requires specially designed experiments.

This paper presents the dynamic analysis of a parallel upper limb rehabilitation robot, which aims to identify the dynamic parameters and implement the model-based control algorithms. For identification purpose, smooth velocities and accelerations are computed by the Kalman filter based on the measured joint angles, and then we apply genetic algorithm (GA) to estimate the base dynamic parameters. Compared with the least square estimation (LSE) method, GA improves significantly accuracy by considering nonlinear frictions in different directions of motion, which is validated by experiments. For the model-based control, we build a PD computed-torque controller for passive training, and the experimental results validate the controller design.

The remaining parts of this paper are organized as follows: Section II presents dynamics modeling of the robot; Section

*This work is partially supported by National Natural Science Foundation of China (Grants #61603386, U1613228, 61533016, 61421004), Early Career Development Award of SKLMCCS, and Beijing Science and Technology Project (Grant No. Z161100001516004).

All author are with the State Key Laboratory of Management and Control for Complex Systems, Institute of Automation, Chinese Academy of Sciences, Beijing, China. Emails: {wangchen2016, liang.peng, luolincong2014, zengguang.hou(corresponding author), weiqun.wang}@ia.ac.cn

978-1-5090-6017-7/18/$31.00 ©2018 IEEE

III compares the LSE-based method and GA-based identification, and verifies the presented approach through experiments. Section IV discusses the model-based robot control of the developed identification model. Some conclusion remarks are finally included in Section V.

II. Robot Introduction and Dynamics Modeling

A. Introduction of the Rehabilitation Robot

In this study, a novel upper limb rehabilitation robot is used, which adopts a five-bar parallel structure as shown in Fig. 1, and its technical specifications are shown in Table I.

TABLE I
TECHNICAL SPECIFICATIONS

Items	Characteristics
DOF	2
Actuation	2 DC motors
Sensors	2 rotary encoders
Range of Joint Motion	-20°∼80°, 80°∼190°
Workspace	600 mm * 450 mm
Motor Torque	∼ 844 mNm
Reduction Ratio	5:1
Force Capability	>20 N

Parallel mechanism has many advantages over its serial counterparts such as high stiffness, simple joint design, low inertial etc [4]. Different from the symmetrical structure and cable driven design of CASIA-ARM [5], this robot has a parallelogram structure with a highly backdrivable belt transmission, which is beneficial to reduce the size of movement linkages and easy maintenance.

As shown in Fig. 1, five revolute joints connect the links of the robot to form a closed chain mechanism, where only two joints at the base are actuated by DC motors, and the others are passive. The patient arm is coupled with the robot at the end-effector and achieves 2-DOF movements in the horizontal plane. With the ability of force feedback, the robot can provide specially designed force fields for the patient in a virtual reality environment. Its dynamics modeling is still needed for advanced model-based control and high-transparency haptic interaction.

B. Modeling of Robot Dynamics

Dynamic analysis of parallel robots is more complex than serial robots for the kinematic constraints between joints [6]. The robot is simplified as a five-bar parallel mechanism as shown in Fig. 2. Link 2 and link 4 are both parallel and equal in length. In this way the closed path in the figure is in fact a parallelogram, which greatly simplifies the computations. Even though there are four articulated links connected through five joints, only two are independent active joints identified as q_1 and q_2.

The Lagrange-based dynamics modeling procedure [7] are as follows:

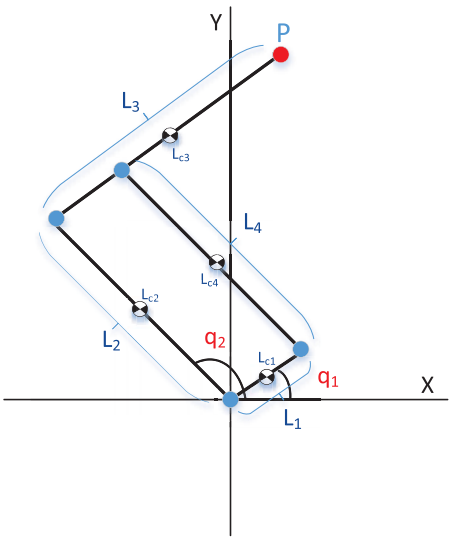

Fig. 2. Five-bar parallel mechanism, where the two joints at the base q_1 and q_2 are coaxial in implementation.

Step 1: The coordinates of the mass center of four articulated links are as below:

$$\begin{aligned}
\begin{bmatrix} x_{c1} \\ y_{c1} \end{bmatrix} &= \begin{bmatrix} l_{c1}\cos q_1 \\ l_{c1}\sin q_1 \end{bmatrix} \\
\begin{bmatrix} x_{c2} \\ y_{c2} \end{bmatrix} &= \begin{bmatrix} l_{c2}\cos q_2 \\ l_{c2}\sin q_2 \end{bmatrix} \\
\begin{bmatrix} x_{c3} \\ y_{c3} \end{bmatrix} &= \begin{bmatrix} l_2\cos q_2 + l_{c3}\cos q_1 \\ l_2\sin q_2 + l_{c3}\sin q_1 \end{bmatrix} \\
\begin{bmatrix} x_{c4} \\ y_{c4} \end{bmatrix} &= \begin{bmatrix} l_1\cos q_1 + l_{c4}\cos q_2 \\ l_1\sin q_1 + l_{c4}\sin q_2 \end{bmatrix},
\end{aligned} \tag{1}$$

and the linear velocities are:

$$\begin{aligned}
v_{c1} &= \begin{bmatrix} -l_{c1}\sin q_1 & 0 \\ l_{c1}\cos q_1 & 0 \end{bmatrix} \dot{q} \\
v_{c2} &= \begin{bmatrix} 0 & -l_{c2}\sin q_2 \\ 0 & l_{c2}\cos q_2 \end{bmatrix} \dot{q} \\
v_{c3} &= \begin{bmatrix} -l_{c3}\sin q_1 & -l_2\sin q_2 \\ l_{c3}\cos q_1 & l_2\cos q_2 \end{bmatrix} \dot{q} \\
v_{c4} &= \begin{bmatrix} -l_1\sin q_1 & -l_{c4}\sin q_2 \\ l_1\cos q_1 & l_{c4}\cos q_2 \end{bmatrix} \dot{q},
\end{aligned} \tag{2}$$

where $q = \begin{bmatrix} q_1 & q_2 \end{bmatrix}$.

Then it is easy to obtain the velocity Jacobians as:

$$\begin{aligned}
J_{v_{c1}} &= \begin{bmatrix} -l_{c1}\sin q_1 & 0 \\ l_{c1}\cos q_1 & 0 \end{bmatrix} \\
J_{v_{c2}} &= \begin{bmatrix} 0 & -l_{c2}\sin q_2 \\ 0 & l_{c2}\cos q_2 \end{bmatrix} \\
J_{v_{c3}} &= \begin{bmatrix} -l_{c3}\sin q_1 & -l_2\sin q_2 \\ l_{c3}\cos q_1 & l_2\cos q_2 \end{bmatrix} \\
J_{v_{c4}} &= \begin{bmatrix} -l_1\sin q_1 & -l_{c4}\sin q_2 \\ l_1\cos q_1 & l_{c4}\cos q_2 \end{bmatrix}.
\end{aligned} \tag{3}$$

Step 2: The angular velocities of the four links are given by

$$\begin{aligned}\omega_1 &= \omega_3 = \dot{q}_1 k \\ \omega_2 &= \omega_4 = \dot{q}_2 k,\end{aligned} \tag{4}$$

where k is the direction vector of the angular velocities.

According to the Euler-Lagrange equation, the inertia matrix is obtained:

$$D(q) = \sum_{i=1}^{4} m_i J_{v_{ci}}^T J_{v_{ci}} + \begin{bmatrix} I_1 + I_3 & 0 \\ 0 & I_2 + I_4 \end{bmatrix}. \tag{5}$$

Substituting (3) into (5), gives

$$\begin{aligned} d_{11}(q) &= m_1 l_{c1}^2 + m_3 l_{c3}^2 + m_4 l_1^2 + I_1 + I_3 \\ d_{12}(q) &= d_{21}(q) = (m_3 l_2 l_{c3} + m_4 l_1 l_{c4}) \cos(q_2 - q_1) \\ d_{22}(q) &= m_2 l_{c2}^2 + m_3 l_2^2 + m_4 l_{c4}^2 + I_2 + I_4, \end{aligned} \tag{6}$$

hence the inertia matrix D is given simply by

$$D = \begin{bmatrix} d_{11}(q) & d_{12}(q) \\ d_{21}(q) & d_{22}(q) \end{bmatrix}.$$

The Christoffel symbols are defined as:

$$c_{ijk} := \frac{1}{2}\left\{ \frac{\partial d_{kj}}{\partial q_i} + \frac{\partial d_{ki}}{\partial q_j} - \frac{\partial d_{ij}}{\partial q_k} \right\}.$$

Substituting for the various quantities in this equation leads to

$$\begin{aligned} c_{111} &= \tfrac{1}{2}\tfrac{\partial d_{11}}{\partial q_1} = 0 \\ c_{121} &= c_{211} = \tfrac{1}{2}\tfrac{\partial d_{11}}{\partial q_2} = 0 \\ c_{122} &= c_{212} = \tfrac{1}{2}\tfrac{\partial d_{22}}{\partial q_1} = 0 \\ c_{221} &= \tfrac{\partial d_{12}}{\partial q_2} - \tfrac{1}{2}\tfrac{\partial d_{22}}{\partial q_1} = \\ &\quad -(m_3 l_2 l_{c3} + m_4 l_1 l_{c4}) \sin(q_2 - q_1) \\ c_{112} &= \tfrac{\partial d_{21}}{\partial q_1} - \tfrac{1}{2}\tfrac{\partial d_{11}}{\partial q_2} = \\ &\quad -(m_3 l_2 l_{c3} + m_4 l_1 l_{c4}) \sin(q_1 - q_2) \\ c_{222} &= \tfrac{1}{2}\tfrac{\partial d_{22}}{\partial q_2} = 0. \end{aligned} \tag{7}$$

Step 3: Applying the Euler-Lagrange equations with respect to all joints:

$$\sum_j d_{kj}(q)\ddot{q}_j + \sum_{i,j} c_{ikj}(q)\dot{q}_i\dot{q}_j + \phi_k(q) = \tau_k, \quad k = 1, 2.$$

Since the robot moves in the horizontal plane, the potential energy remains unchanged, hence $\phi_k = 0$. The dynamic equations can be obtained :

$$\begin{aligned} d_{11}\ddot{q}_1 + d_{12}\ddot{q}_2 + c_{221}\dot{q}_2^2 + \varphi_1 &= \tau_1 \\ d_{21}\ddot{q}_1 + d_{22}\ddot{q}_2 + c_{112}\dot{q}_1^2 + \varphi_2 &= \tau_2. \end{aligned} \tag{8}$$

In this case the centripetal and Coriolis matrix is given as:

$$C = \begin{bmatrix} 0 & h\dot{q}_2 \\ -h\dot{q}_1 & 0 \end{bmatrix}, \tag{9}$$

where

$$h = -(m_3 l_2 l_{c3} + m_4 l_1 l_{c4}) \sin(q_2 - q_1).$$

Step 4: The dynamic equations of the robot can be expressed in the following form:

$$D(q)\ddot{q} + C(q, \dot{q})\dot{q} = \tau. \tag{10}$$

By considering the traditional joint friction model in [8], the obtained dynamic model is given by

$$D(q)\ddot{q} + C(q, \dot{q})\dot{q} + \tau_f = \tau, \tag{11}$$

where

$$\tau_f = K_v\dot{q} + K_c \mathrm{sgn}(\dot{q})$$

with K_v and K_c the coefficient matrix representing the terms of viscous friction and Coulomb friction, which are defined respectively by:

$$K_v = \begin{bmatrix} k_{v1} & 0 \\ 0 & k_{v2} \end{bmatrix},\ K_c = \begin{bmatrix} k_{c1} & 0 \\ 0 & k_{c2} \end{bmatrix}.$$

For ease of identification of the unknown dynamic parameters, the robot dynamic model can be rearranged into a linear form with respect to these parameters:

$$Y(q, \dot{q}, \ddot{q})\Phi = \tau, \tag{12}$$

where $Y(q, \dot{q}, \ddot{q})$ is a 2×7 observation matrix whose element in the i^{th} row and j^{th} column is $Y_{i,j}$, and Φ is a 7×1 vector containing the unknown dynamic parameter ϕ_i.

The elements in $Y(q, \dot{q}, \ddot{q})$ and Φ are given by (13) and (14).

$$\begin{cases} Y_{1,1} = \ddot{q}_1 \\ Y_{1,2} = \ddot{q}_2 \cos(q_2 - q_1) + \dot{q}_2^2 \sin(q_1 - q_2) \\ Y_{1,4} = \dot{q}_1 \\ Y_{1,5} = \mathrm{sgn}(\dot{q}_1) \\ Y_{2,2} = \ddot{q}_1 \cos(q_2 - q_1) + \dot{q}_1^2 \sin(q_2 - q_1) \\ Y_{2,3} = \ddot{q}_2 \\ Y_{2,6} = \dot{q}_2 \\ Y_{2,7} = \mathrm{sgn}(\dot{q}_2) \end{cases} \tag{13}$$

$$\begin{cases} \phi_1 = m_1 l_{c1}^2 + m_3 l_{c3}^2 + m_4 l_1^2 + I_1 + I_3 \\ \phi_2 = m_3 l_2 l_{c3} + m_4 l_1 l_{c4} \\ \phi_3 = m_2 l_{c2}^2 + m_3 l_2^2 + m_4 l_{c4}^2 + I_2 + I_4 \\ \phi_4 = k_{v1} \\ \phi_5 = k_{c1} \\ \phi_6 = k_{v2} \\ \phi_7 = k_{c2} \end{cases} \tag{14}$$

III. Parameter Identification and Experiments

A. Estimation of Joint Velocity and Acceleration

Calculation of the observation matrix in (13) requires estimations of the joint velocities and accelerations. Since the robot is only equipped with position sensors, we can obtain the joint velocities and accelerations by numerically differentiating the joint position. However, the derivative, and especially the second derivative, of a set of data are inherently noisy because the differentiator essentially behaves like a high-pass filter [9]. A solution to this problem is to filter the velocity and acceleration signals using the Kalman filter.

In this study, the following linear discrete-time model is used for each joint:

$$\begin{aligned} x_k &= Gx_{k-1} + \omega_{k-1}, \omega \sim N(0, Q) \\ y_k &= Cx_k + v_k, v \sim N(0, R), \end{aligned} \tag{15}$$

where

$$x_k = \begin{bmatrix} q_k & \dot{q}_k & \ddot{q}_k \end{bmatrix}^T,$$

$$G = \begin{bmatrix} 1 & T_s & \frac{1}{2}{T_s}^2 \\ 0 & 1 & T_s \\ 0 & 0 & 1 \end{bmatrix},$$

$$C = \begin{bmatrix} 1 & 0 & 0 \end{bmatrix},$$

and y is the actual position signal; ω and v are the systematic noise and measurement noise, respectively.

Five formulas are utilized to implement Kalman filter:

$$\begin{cases} \hat{x}(k|k-1) = G\hat{x}(k-1|k-1) \\ P(k|k-1) = GP(k-1|k-1)G^T + Q \\ K = \frac{P(k|k-1)C^T}{CP(k|k-1)C^T + R} \\ \hat{x}(k|k) = \hat{x}(k|k-1) + K(Z(k) - C\hat{x}(k|k-1)) \\ P(k|k) = (I - KC)P(k|k-1). \end{cases} \tag{16}$$

Firstly, the current state is predicted according to the last step. Next, the estimated covariance is calculated based on the state and the systematic noise covariance Q, and the Kalman gain K is caculated according to the covariance matrix and the measurement noise covariance R. Finally, the filtered velocities and accelerations are calculated in term of the Kalman gain, the predicted state and the measurement, and then the estimation error covariance matrix is calculated for next step.

B. LSE Parameter Identification

By considering the linear relationship of robot dynamics with respect to unknown parameters as in (12), LSE method is tested firstly for parameter identification.

By making use of the inverse dynamic model, the following overdetermined linear system of equations in Φ is obtained:

$$Y_s\Phi = \tau_s + \varepsilon, \tag{17}$$

where Y_s is a 2M $\times$ 7 observation matrix, τ_s is a 2M $\times$ 1 torque observation vector, ε is a residual error vector, M is the number of the sampled points; and Y_s and τ_s are defined respectively by:

$$Y_s = [Y^T(q(1), \dot{q}(1), \ddot{q}(1)) \cdots Y^T(q(M), \dot{q}(M), \ddot{q}(M))]^T \tag{18}$$

and

$$\tau_s = [\tau^T(1) \cdots \tau^T(M)]^T, \tag{19}$$

where $\tau(i)$ represents the i^{th} measured torque; the elements of $Y(q(i), \dot{q}(i), \ddot{q}(i))$ are functions of the joint angles $q(i)$, angular velocities $\dot{q}(i)$ and accelerations $\ddot{q}(i)$.

Since Y_s and τ_s can be obtained by (18) and (19), the undetermined parameters can be identified by LSE:

$$\hat{\Phi} = ({Y_s}^T Y_s)^{-1} {Y_s}^T \tau_s, \tag{20}$$

where $\hat{\Phi}$ represents the estimated value of dynamic parameters.

C. Experiments

In this study, reaching movement trajectory is selected for identifying the dynamic parameters, which is a most used trajectory in rehabilitation training.

Through a large number of observations, the actual trajectory generated by taking reaching actions between two points satisfies the Minimum jerk condition:

$$\begin{aligned} &\tfrac{x(t)-x_i}{x_d-x_i} = \tfrac{y(t)-y_i}{y_d-y_i} = \\ &10(\tfrac{t}{t_d})^3 - 15(\tfrac{t}{t_d})^4 + 6(\tfrac{t}{t_d})^5, \end{aligned} \tag{21}$$

where (x_i, y_i) and (x_d, y_d) are respectively the coordinates of starting point and ending point, t_d is the total movement time. The trajectory of 5-order polynomial form corresponds to a straight line connecting two points.

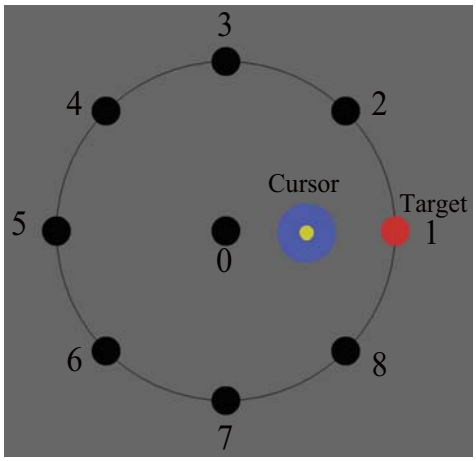

Fig. 3. Reaching movement task in the experiment.

Fig. 3 shows the actual trajectory in the workspace of the robot. There are 8 target points on the circle edge, and target 0 is at the center of the circle.

Under the excitation of above trajectories based on simple PID joint control, the robot achieves autonomous motions between target 0 and 8 targets around the circle (the radius is 0.2 m) [10]. The sampling frequency is 50Hz, and the joint torques and angles are recorded at the same time. Two experiments have been carried out: experiment for parameter estimation and experiment for model validation.

1) Data Processing: Ten periods of data were recorded and the first and last periods were neglected. Firstly, a zero phase filter was utilized to preprocess the measured torques. Next, in order to obtain exact calculation of the joint velocities and accelerations, the angles of two joints were fed into Kalman filter respectively. Since the joint angles were measured by two encoders mounted on the motor shafts and the variations were relatively small, the derived velocities and accelerations can be considered accurate. Finally, the preprocessed dataset was divided into two parts, the motion data containing target 1, 2, 3, 4 was used as the training set and the remaining data used as the validation set.

2) Parameter Estimation: The robot model contains three barycentric parameters and four friction parameters (viscous and Coulomb friction parameters for two joints), which are defined by (14). Based on the joint torques, angles, velocities and accelerations in training set, the observation matrix Y_s and torque observation vector τ_s were obtained. These model parameters defined by (12) can be estimated by the LSE method, which identification procedure was discussed in Section III-B. The results are given in Table II.

TABLE II
PARAMETERS ESTIMATED BY LSE METHOD

Parameter	Value	Parameter	Value
$\hat{\phi}_1(\mathrm{kgm}^2)$	0.0593	$\hat{\phi}_5(\mathrm{Nm})$	0.1209
$\hat{\phi}_2(\mathrm{kgm}^2)$	0.1609	$\hat{\phi}_6(\mathrm{kgm}^2/\mathrm{s})$	0.2637
$\hat{\phi}_3(\mathrm{kgm}^2)$	0.2380	$\hat{\phi}_7(\mathrm{Nm})$	0.1704
$\hat{\phi}_4(\mathrm{kgm}^2/\mathrm{s})$	0.2028		

3) Model Validation: The validation of the obtained parameter estimations is achieved by comparing the measured torques and estimations of these torques based on the validation data of different trajectories.

The estimated torques of the validation samples are calculated by:

$$\tau_{est} = Y_s(q, \dot{q}, \ddot{q})\hat{\Phi}, \tag{22}$$

where $Y_s(q, \dot{q}, \ddot{q})$ is the observation matrix, depending on the recorded angles, as well as the angular velocities and accelerations derived from Kalman filter.

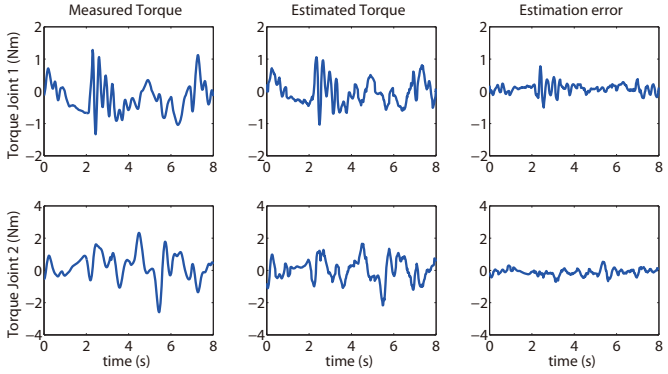

Fig. 4. Model validation results of LSE-based parameter identification

Fig. 4 shows the results of the measured torques, estimated torques and the corresponding estimation errors. The results of the errors and the measured torques denote that the model we obtained is capable of estimating thel torque. However, the estimation error for low joint angular velocity is relatively big, which indicates that the assumed friction model in (11), is too simple to capture the complex dynamic friction behavior. Besides, LSE method is unable to achieve consistent and unbiased estimation when there is colored noise in the system, and GA are used in the study to solve these problems.

D. GA-based Parameter Identification

GA is a parallel and global search optimization technique based on natural selection mechanism [11]-[12]. It is not limited by assumptions about the search space, and can be applied to various problems. A simple genetic algorithm uses three basic genetic operators: reproduction, crossover and mutation. In order to distinguish nonlinear frictions in different directions of motion, friction parameters in (14) are redefined respectively by:

$$\begin{cases} \phi_4 = k_{v1\_pos} & \phi_4{}' = k_{v1\_neg} \\ \phi_5 = k_{c1\_pos} & \phi_5{}' = k_{c1\_neg} \\ \phi_6 = k_{v2\_pos} & \phi_6{}' = k_{v2\_neg} \\ \phi_7 = k_{c2\_pos} & \phi_7{}' = k_{c2\_neg}. \end{cases} \tag{23}$$

The proposed identification algorithm by GA is as follows.

1) Initialize *h* chromosomes as population by real-value encoding, where *h*=30 is the size of population.
2) Calculate the fitness values for *h* chromosomes.
3) Based on the fitness of each individual, the best chromosome in this generation is selected through the selection process.
4) Reproduction and formation of the new generation.
5) Crossover all chromosomes under the probability P_c, and generate new *h* offsprings.
6) Calculate the fitness values for all 2*h* chromosomes and preserve *h* chromosomes by elite strategy.
7) Mutate all chromosomes under the probability P_m, and generate new *h* offsprings.
8) Calculate the fitness values for all 2*h* chromosomes and preserve *h* chromosomes by elite strategy.
9) Go to 2) and 3).
10) If the generation number is enough or fitness satisfies the criterion, end identification process. If not, repeat from 4).

The objective function used in 2), 6) and 8) is expressed:

$$\begin{aligned} \tau_{est} &= Y_s(q, \dot{q}, \ddot{q})\hat{\Phi}, \\ \varepsilon_{RMS} &= \sqrt{\frac{1}{M}\sum_{m=1}^{M}(\tau_s(m) - \tau_{est}(m))^2}. \end{aligned} \tag{24}$$

By considering the convergence under the practical computation load, the number of chromosomes in the population is 30. The mutation rate P_m is chosen according to the population size, and then the search is prevented to be a random one. GA-based parameter identification experiments has been performed in the same way as discussed above.

As the result of 100 generations of generic process, the estimated parameters are listed in Table III, and Fig. 5 gives the comparison between the measured torques and the estimated torques for model validation.

As shown in Table III, $\hat{\phi}_4$ and $\hat{\phi}_4'$ are almost the same, so are $\hat{\phi}_6$ and $\hat{\phi}_6'$. It can be deduced that the non-linear Coulomb term is the main factor contributing to large estimation errors at low velocities. For simplicity, the final dynamic model only has 9 parameters, where two viscous friction estimating parameters

TABLE III
11 PARAMETERS ESTIMATED BY GA

Parameter	Value	Parameter	Value
$\hat{\phi}_1(\mathrm{kgm}^2)$	0.0744	$\hat{\phi}_5(\mathrm{Nm})$	0.0082
$\hat{\phi}_2(\mathrm{kgm}^2)$	0.1843	$\hat{\phi}'_5(\mathrm{Nm})$	0.2580
$\hat{\phi}_3(\mathrm{kgm}^2)$	0.2390	$\hat{\phi}_6(\mathrm{kgm}^2/\mathrm{s})$	0.4776
$\hat{\phi}_4(\mathrm{kgm}^2/\mathrm{s})$	0.2202	$\hat{\phi}'_6(\mathrm{kgm}^2/\mathrm{s})$	0.5482
$\hat{\phi}'_4(\mathrm{kgm}^2/\mathrm{s})$	0.2644	$\hat{\phi}_7(\mathrm{Nm})$	0.2446
		$\hat{\phi}'_7(\mathrm{Nm})$	0.0036

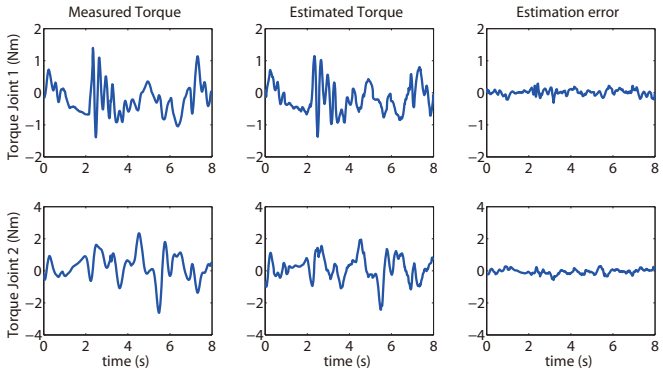

Fig. 5. Model validation results of GA-based parameter identification

are left no matter the velocity directions. The results of 9 parameters GA-based identification are listed in Table IV.

TABLE IV
9 PARAMETERS ESTIMATED BY GA

Parameter	Value	Parameter	Value
$\hat{\phi}_1(\mathrm{kgm}^2)$	0.0776	$\hat{\phi}_5(\mathrm{Nm})$	0.0222
$\hat{\phi}_2(\mathrm{kgm}^2)$	0.1843	$\hat{\phi}'_5(\mathrm{Nm})$	0.2807
$\hat{\phi}_3(\mathrm{kgm}^2)$	0.2297	$\hat{\phi}_6(\mathrm{kgm}^2/\mathrm{s})$	0.5518
$\hat{\phi}_4(\mathrm{kgm}^2/\mathrm{s})$	0.1880	$\hat{\phi}_7(\mathrm{Nm})$	0.2073
		$\hat{\phi}'_7(\mathrm{Nm})$	0.0054

In order to compare the accuracy of identification results in Table II, Table III and Table IV, the RMS error of the estimated torques is defined as:

$$\tau_{rmse} = \sqrt{\frac{1}{K}\sum_{k=1}^{K}(\tau_{est,k} - \tau_{s,k})^2}, \tag{25}$$

where K is the size of validation set, $\tau_{est,k}$ and $\tau_{s,k}$ are respectively the kth estimated and measured torques for each joint. Table V shows the RMS of the estimation errors for LSE-based, 9 parameters GA-based and 11 parameters GA-based validation experiments. It can be seen that, the GA-based method improves significantly accuracy for parameter identification.

TABLE V
RMS OF THE ESTIMATION ERROR

	LSE method	GA_9para	GA_11para
joint1	0.1163 N-m	0.0358 N-m	0.0346 N-m
joint2	0.2006 N-m	0.1017 N-m	0.1019 N-m

When the system is contaminated by colored noise, the LSE method fails to give the unbiased estimation, and GA yields better identification result. Through parameterizing the the nonlinearity of friction, GA is utilized to optimize the combination of 9 parameters. Each individual in the population is feasible solution for parameter identification, and the elite preservation policy is applied to ensure algorithm evolve towards the optimal direction. Despite modeling errors (mechanical losses in the actuators and the efficiency of the transmissions), the estimated models are accurate but biased. Extending the robot model to include more advanced friction models is expected to improve the prediction accuracy.

IV. MODEL-BASED ROBOT CONTROL

For the purpose of validation, PD computed-torque control experiment is conducted, which is the basis for passive training. The objective of this experiment is to force joint variables $q = \begin{bmatrix} q_1 & q_2 \end{bmatrix}^T$ to track circular passive training trajectories, and the the desired trajectories of the robot are:

$$\begin{aligned} x_d(t) &= R\cos(\tfrac{2\pi}{T_d}t) \\ y_d(t) &= 0.4 + R\sin(\tfrac{2\pi}{T_d}t). \end{aligned} \tag{26}$$

where R = 0.2 m is the radius, and T_d = 7.2 s is the period.

Computed Torque Control (CTC) is a special application of feedback linearization of nonlinear systems. Briefly speaking, by modeling the robot inertia (as well as centripetal and Coriolis forces) characteristics, CTC can be used to linearize robotic dynamics and achieve the compensation for the changing robotic dynamics. A block diagram of the PD computed-torque controller appears in Fig. 6.

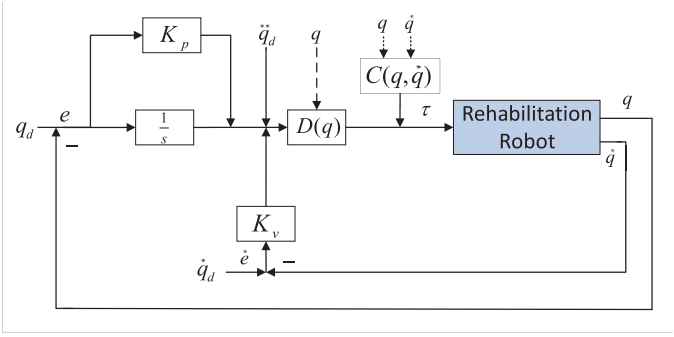

Fig. 6. Block diagram of the PD computed-torque controller

It is supposed that the desired trajectory $q_d(t)$ has been selected for the robot motion. The dynamic equations of the robot can be expressed as

$$D(q)\ddot{q} + C(q,\dot{q})\dot{q} + \tau_d = \tau, \tag{27}$$

where $q = \begin{bmatrix} q_1 & q_2 \end{bmatrix}^T$, $\tau = \begin{bmatrix} \tau_1 & \tau_2 \end{bmatrix}^T$ is the arm control torque, τ_d is the disturbance torque, $e = q_d - q$ is defined as trajectory tracking error vectors.

Defining the control input function as proportional-plus derivative (PD) feedback:

$$u = -K_v\dot{e} - K_p e, \tag{28}$$

and substituting (28) into the computed-torque control law [13] yields

$$\tau = D(q)(\ddot{q}_d + K_v\dot{e} + K_p e) + C(q,\dot{q})\dot{q}, \tag{29}$$

where K_p and K_v are proportional and derivative constant matrices, respectively. Substituting (29) into (27), we have

$$\ddot{e} = -K_v\dot{e} - K_p e + D^{-1}(q)\tau_d. \tag{30}$$

Therefore, the tracking error will asymptotically converge to zero for any desired trajectory in absence of disturbances τ_d.

The designed parameters in PD computed-torque controller are selected as:

$$K_p = \begin{bmatrix} 100 & 0 \\ 0 & 100 \end{bmatrix}, \; K_v = \begin{bmatrix} 5 & 0 \\ 0 & 5 \end{bmatrix}.$$

The tracking results in X and Y directions are shown in Fig. 7, where the actual trajectories and desired trajectories almost overlap each other, and smaller tracking errors can be acquired by adjusting K_p and K_v. Thus, it is safely said that PD computed-torque controller exhibits good tracking performances based on the dynamic model obtained in Section III-D.

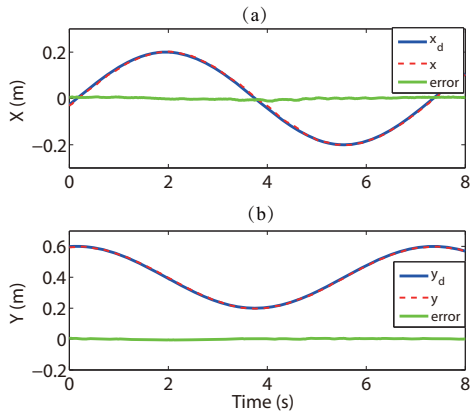

Fig. 7. Desired and actual trajectories, and tracking errors in X,Y directions

V. Conclusion

This paper presents the dynamics modeling and control method of a novel upper limb rehabilitation robot, which are validated by experiments. For the purpose of dynamic parameter identification, smooth joint velocities and accelerations are computed by Kalman filter, and then GA is utilized to estimate the dynamic parameters. Compared with the LSE-based parameter identification, GA yields precise identification results by considering nonlinear frictions in different direction of velocity. Further, a PD computed-torque controller is designed and an experiment of circular path passive training task is conducted to validate the effectiveness of this method.

References

[1] L. Peng, Z.-G. Hou, L. Peng, L. Luo, and W. Wang, "Robot assisted rehabilitation of the arm after stroke: prototype design and clinical evaluation," *Science China Information Sciences*, vol. 60, no. 7, p. 073201, 2017.

[2] L. Peng, Z.-G. Hou, N. Kasabov, L. Peng, J. Hu, and W. Wang, "Implementation of active training for an upper-limb rehabilitation robot based on impedance control," in *Proceedings of 27th Chinese Control and Decision Conference (CCDC)*, 2015, pp. 5453–5458.

[3] J. Swevers, C. Ganseman, D. B. Tukel, J. De Schutter, and H. Van Brussel, "Optimal robot excitation and identification," *IEEE transactions on robotics and automation*, vol. 13, no. 5, pp. 730–740, 1997.

[4] G. Campion, "The pantograph mk-ii: a haptic instrument," in *The Synthesis of Three Dimensional Haptic Textures: Geometry, Control, and Psychophysics*. Springer, 2005, pp. 45–58.

[5] L. Peng, Z.-G. Hou, L. Peng, and W. Wang, "Design of casia-arm: A novel rehabilitation robot for upper limbs," in *Proceedings of IEEE/RSJ International Conference on Intelligent Robots and Systems (IROS)*, 2015, pp. 5611–5616.

[6] L. Peng, Z.-G. Hou, and W. Wang, "Dynamic modeling and control of a parallel upper-limb rehabilitation robot," in *Proceedings of IEEE International Conference on Rehabilitation Robotics (ICORR)*, 2015, pp. 532–537.

[7] M. W. Spong and M. Vidyasagar, *Robot dynamics and control*. John Wiley & Sons, 2008.

[8] M. Grotjahn, M. Daemi, and B. Heimann, "Friction and rigid body identification of robot dynamics," *International Journal of Solids and Structures*, vol. 38, no. 10, pp. 1889–1902, 2001.

[9] W. Khalil and E. Dombre, *Modeling, Identification and Control of Robots*, pp. 291–311, 2004.

[10] L. Peng, Z. G. Hou, and W. Q. Wang, "Synchronous active interaction control and its implementation for a re-habilitation robot," *Acta Automatica Sinica*, vol. 41, no. 11, pp. 1837–1846, 2015.

[11] K.-S. Tang, K.-F. Man, S. Kwong, and Q. He, "Genetic algorithms and their applications," *IEEE signal processing magazine*, vol. 13, no. 6, pp. 22–37, 1996.

[12] K.-F. Man, K.-S. Tang, and S. Kwong, "Genetic algorithms: concepts and applications in engineering design," *IEEE transactions on Industrial Electronics*, vol. 43, no. 5, pp. 519–534, 1996.

[13] F. L. Lewis, D. M. Dawson, and C. T. Abdallah, *Robot manipulator control: theory and practice*. CRC Press, 2003.